Tribology International 200 (2024) 110183

Contents lists available at ScienceDirect

Tribology International

journal homepage: www.elsevier.com/locate/triboint

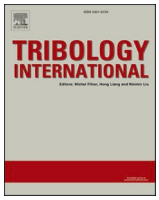

Synergistic effects of nitrogen-containing functionalized copolymer and silicon-doped DLC for friction and wear reduction

Takeru Omiya [a,b,c,*], Enrico Pedretti [d], Manuel Evaristo [a], Albano Cavaleiro [a,c], Arménio C. Serra [b], Jorge F.J. Coelho [b,c], Fabio Ferreira [a,c], Maria Clelia Righi [d,**]

[a] University of Coimbra, CEMMPRE, ARISE, Department of Mechanical Engineering, Rua Luís Reis Santos, 3030–788 Coimbra,. Portugal
[b] University of Coimbra, CEMMPRE, ARISE, Department of Chemical Engineering, Rua Silvio Lima, 3030–790 Coimbra, Portugal
[c] Laboratory for Wear, Testing & Materials, Instituto Pedro Nunes, Rua Pedro Nunes, 3030–199 Coimbra, Portugal
[d] Department of Physics and Astronomy, University of Bologna, Bologna 40127 Italy

ARTICLE INFO

Keywords:
Si-doped DLC
Functionalized copolymer
Ab initio calculation
Molecular adsorption

ABSTRACT

We present a strategy to enhance the tribological performances of diamond-like carbon (DLC) films based on synergistic chemical modifications in the polymer lubricant additives and in the carbon film. Our experiments revealed that the polymer functionalization with nitrogen-containing groups and the DLC doping with silicon atoms result in significant friction and wear reduction under severe boundary lubrication conditions. Atomic Force Microscopy revealed the formation of a lubricious tribofilm. Ab initio calculations highlighted the key role of N-Si interactions in promoting the polymer chemisorption on the film, which represents the first, essential step for the tribofilm formation. Our findings suggest that targeted chemical modifications in lubricants and films can substantially advance the tribological performances of DLC films for various industrial applications.

1. Introduction

Polymers can be used as additives to base oil with several advantages, including environment sustainability, low friction coefficients, excellent load-carrying capacity, and the ability to reduce wear and prevent surface damage [1]. The unique role of polymers in lubrication is further amplified when they have specific side groups to possess precise characteristics that enhance their performance on steel surfaces, making them highly suitable for applications in numerous industrial sectors [2–6]. Functionalized copolymers, in particular, have garnered significant attention owing to their exceptional tribological properties [7,8]. These copolymers are synthesized by incorporating specific functional side groups into the polymer backbone, imparting them with tailored reactivity [8]. By judiciously selecting the functional groups, these copolymers can reduce wear and friction effectively, improving tribological performance on steel surfaces [9,10]. Moreover, the absence of metal in this copolymer eliminates the issue of diesel particulate filter clogging often encountered with zinc dialkyldithiophosphates (ZnDTP), a conventional anti-wear agent [11].

While functionalized copolymers have demonstrated remarkable potential, diamond-like carbon (DLC) films that have captured the automotive industry's attention for their superior abilities to reduce wear and friction [12–16]. Thus, to create a lubrication system that combines DLC and additives, some studies were conducted to determine the synergistic effect of DLC and ZnDTP, as well as the friction-reducing effect of glycerol mono-oleate on DLC [17,18]. However, the low reactivity of conventional lubricants and polymers with DLC films presents a significant challenge in achieving optimal lubrication performance [14,19]. To address this challenge, researchers have explored doped DLCs, where specific elements or compounds are introduced to modify the surface properties and enhance reactivity [20,21]. These doped DLCs offer numerous advantages, such as improved adhesion, reduced friction, enhanced wear resistance, and increased compatibility with lubricants and polymers [22–26]. Among various doped DLC films, silicon-doped DLC (Si-DLC) film has demonstrated exceptional potential due to its unique properties, including excellent tribological performance, increased surface reactivity, and strong interfacial adhesion [27].

Previous *ab initio* molecular dynamics simulations by our group showed that Si dopants improve the tribological performances of DLC in

* Corresponding author at: University of Coimbra, CEMMPRE, ARISE, Department of Mechanical Engineering, Rua Luís Reis Santos, 3030–788 Coimbra, Portugal.
** Corresponding author.
E-mail addresses: takeru.omiya@student.dem.uc.pt (T. Omiya), clelia.righi@unibo.it (M.C. Righi).

https://doi.org/10.1016/j.triboint.2024.110183
Received 19 July 2024; Received in revised form 21 August 2024; Accepted 29 August 2024
Available online 30 August 2024

humid environments due to the key role played by silicon in enhancing the reaction rate for water molecule dissociation, favoring the surface hydroxylation and thus increasing its hydrophilicity [28,29]. These studies provided insights into the effects of dopants on the wetting properties and friction-reduction performance of carbon-based materials, suggesting that the film composition can be optimized to achieve superior lubrication performance. However, new lubrication systems which combine functionalized copolymers and DLC films have not yet been explored.

Here, we aim to comprehensively investigate the interaction between functionalized copolymers and Si-DLCs in enhancing lubrication performance. The research involves wear and friction measurements, surface analyses, and first principles calculations of the additive-surface reactivity to provide a deep understanding of the microscopic mechanisms and establish a correlation between the molecular structure and composition of functionalized copolymers and their lubricating properties.

2. Experimental

2.1. DLC films

The DLC films were deposited on M2 steel disks with a 50 mm diameter and a hardness of 801 Vickers and 2 cm square monocrystalline Si substrates. In preparation for the deposition process, the steel substrates were subjected to a polishing step using 3 μm diamond paste. This polishing procedure resulted in a surface roughness (*Ra*) of approximately 100 nm for the steel samples. The depositions were performed in a Teer Coatings unbalanced magnetron sputtering system with four cathodes. The targets were powered by direct current (DC) power supplies, and the substrates were subjected to a pulsed DC bias of −50 V. Four targets measuring 380 × 175 mm were utilized: one made of pure chromium, two made of pure graphite, and one made of pure silicon. To improve the adhesion of the film, a 300 nm thick chromium interlayer was deposited before the deposition of DLC film. The DLC deposition process involved maintaining constant power on the two graphite targets while varying the power on the silicon target to control the silicon content in the Si-DLC films. The deposition occurred in an argon atmosphere, with the chamber pressure controlled to maintain appropriate sputtering conditions. The target power applied to the silicon target ranged from 120 W to 350 W, resulting in silicon contents in the coatings from 4.8 at% to 14.4 at%. The duration of the process was adjusted to achieve a consistent coating thickness of approximately 1.0 μm. The process parameters, including the gas flow rate and chamber pressure, were optimized to ensure uniform coating deposition and desired properties. The composition of films was evaluated using scanning electron microscopy (SEM) equipped with energy-dispersive X-ray spectroscopy. The film hardness and Young's modulus were measured using a Nanotest platform from Micromaterials that was equipped with a Berkovich indenter. The measurements were taken at 16 different locations, and the standard deviation was calculated. Table 1 summarizes the designations assigned to the DLC films investigated in this study, along with their corresponding properties. Si-DLC films are recognized for experiencing a decrease in hardness due to reduced residual stress in the phase of low Si concentration and an increase in hardness resulting from SiC formation in higher Si concentrations [27,30,31]. As in previous studies, this study also observes two trends with increasing Si content: up to 10 at% Si content, there is a slight decrease in hardness and Young's modulus remains almost constant. Therefore, the decrease in hardness is related to external factors, such as a decrease in residual stress. Additionally, as the Si content increases, both the hardness and Young's modulus increase.

Table 1
Properties of pure-DLC and Si-DLCs.

DLC Name	Si [at %]	Roughness: R_a [nm]	Hardness [GPa]	Young Modulus [GPa]	sp^3 content [%]
pure-DLC	0	4.9 ± 0.1	15.6 ± 0.6	167 ± 3	26
Si-DLC 4.8 %	4.8	6.7 ± 0.2	14.0 ± 0.9	166 ± 5	30
Si-DLC 8.3 %	8.3	6.4 ± 0.1	12.4 ± 0.5	165 ± 3	42
Si-DLC 14.4 %	14.4	5.2 ± 0.2	19.4 ± 0.6	204 ± 4	56

The morphology of the DLCs was determined by atomic force microscopy (AFM, Innova Veeco). Surface topography was observed using tapping mode, and the lateral signal on the surface was measured using contact mode. All surface topography measurements using tapping and contact mode were performed with the following settings: scan size = 5 μm x 5 μm, scan rate = 1.2 Hz. The lateral signal measurement employed a NANOSENSORS PPP-LFMR cantilever with a force constant of 0.2 N/m.

To gain a deeper understanding of the films' crystal structure at a detailed level, Raman spectroscopy and angle-resolved X-ray photoelectron spectroscopy (ARXPS) were employed. Raman spectroscopy was performed by Renishaw inVia™ confocal Raman microscope. A 532 nm laser was irradiated on the surface with 1800 lines/mm grating with a laser spot size of approximately 1 μm and a power of 50 mW at an acquisition time of 10 s. The spatial resolutions in lateral and axial directions were 0.25 and 1 μm, respectively. Measurements were taken at three different spots. Fig. S1 in the Supplementary Information shows a simultaneous downshift of the G peak and a decrease in the I_D/I_G ratio, indicating a reduction in the average size of graphitic sp^2 bonded clusters and an enhancement of sp^3 bond formation due to the presence of Si [32]. The sp^3 content in the DLC film can be determined using FWHM of G peak [33,34]. The calculated sp^3 content in each DLC film is presented in Table 1.

The ARXPS measurements were conducted within a high-vacuum environment, where the pressure did not exceed 1×10^{-9} mbar, utilizing a hemispherical analyzer (SPECS Phoibos 100 MCD-5). A 9 eV pass energy facilitated a consistent resolution of 0.9 eV. For the calibration of binding energies, the reference lines Au 4 $f_{7/2}$ at 84.0 eV, Ag $3d_{5/2}$ at 368.3 eV, and Cu $2p_{3/2}$ at 932.7 eV were employed. The X-ray source, featuring a dual anode of Mg and Al, was maintained at 300 W, employing Mg Kα radiation ($h\nu = 1253.6$ eV). The sample positioning on a stage with four degrees of mobility allowed the variation of the emission angle from 0° to 50°, enabling the execution of ARXPS analyses. Based on ARXPS measurements using two different angles, it is expected that the thickness of the Si mixed oxide layer covering the Si-DLC is approximately 1.2 nm (Fig. S2 in the Supplementary Information).

2.2. Lubricants

The functionalized copolymers were synthesized according to the outlined procedure, having lauryl methacrylate (LMA) as the alkyl group and 2-dimethylaminoethyl methacrylate (DMAEMA) as the functional group by atom transfer radical polymerization (ATRP) (Fig. 1) [35]. Briefly, copper wire (Cu^0, Alfa Aesar, 99.9 %, 1 mm diameter) and copper (II) bromide (Acros Organics, 99 %) were added to a Schlenk reactor sealed with a rubber septum and purged with nitrogen. A mixture of ethyl-α-bromophenyl acetate (Sigma Aldrich, 97 %), LMA (TCI, 97.0 %), *N,N,N,N,N*-pentamethyldiethylenetriamine (Aldrich, 99 %), and anisole (Sigma Aldrich, 99.0 %) was prepared in a separate round bottom flask and purged with nitrogen for at least 30 min. The reactor was placed in a preheated water bath at T = 50 °C with stirring for 4 h. The DMAEMA (Acros Organics, 99 %) was then added to the Schlenk reactor. The synthesis was stopped after different reaction times depending on the copolymer (Table 2). To evaluate the tribological properties of the functional group, three polymers, non-functionalized

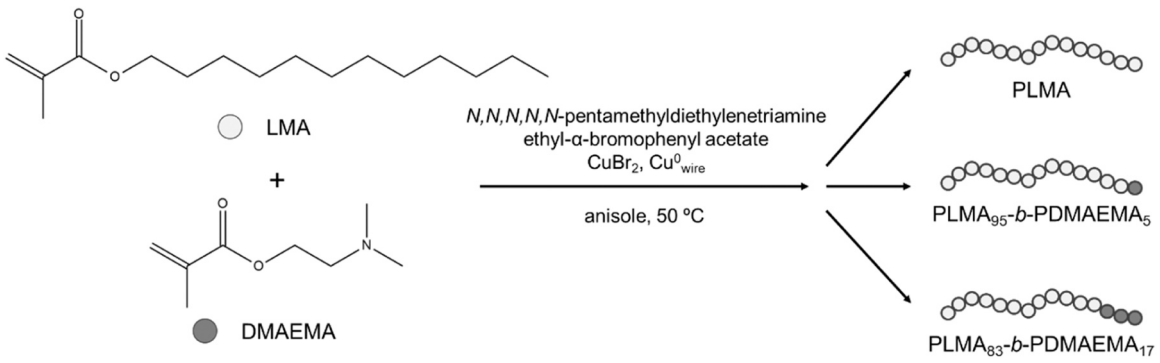

Fig. 1. Chemical structure of PLMA and PLMA-*b*-PDMAEMA prepared by ATRP.

Table 2
Physical properties of synthesized polymers.

Polymer Name	Reaction time of PDMAEMA	PDMAEMA amount [mol%]	M_w [kDa]	M_w/M_n
PLMA	-	0	38	1.07
$PLMA_{95}$-*b*-$PDMAEMA_5$	1 hr	5	38	1.08
$PLMA_{83}$-*b*-$PDMAEMA_{17}$	2 hr	17	34	1.03

PLMA, $PLMA_{95}$-*b*-$PDMAEMA_5$, and $PLMA_{83}$-*b*-$PDMAEMA_{17}$, were synthesized. The amount of DMAEMA in the block copolymer structure was calculated from ^{1}H NMR. The NMR chemical shift of the block copolymer is shown in the Supplementary Information. The final product was isolated by drying overnight at room temperature under airflow. The final yield of the block copolymer was $\geq$ 70 %.

The polyalphaolefin 4 (PAO 4) as the base lubricant with 8 wt% of the polymer was prepared by mixing 8 g of the polymer in 92 g of PAO 4. The kinematic viscosity of the solution at 80 °C was 8.5 mm^2/s. Dynamic light scattering (DLS) was utilized to measure the particle aggregation size of the polymers dissolved in PAO 4 using a particle size analyzer (Zetasizer Nano ZS, Malvern Instruments).

2.3. Tribological tests

Friction tests employing a ball-on-disk tribometer (Rtec MFT-5000) in reciprocating motion were conducted under a load of 3 N, corresponding to a maximum Hertzian contact pressure of 1.0 GPa. The load cell utilized to measure friction has a resolution of 6 mN and can provide a maximum normal force of 200 N. The tribometer was calibrated by the equipment manufacturer, Rtec Instruments. These friction tests were conducted with a frequency range of 5.0 to 0.2 Hz and a stroke length of 15 mm, and each test was repeated at least three times. Before conducting the friction test, a running-in operation was performed for 5 min at a frequency of 3.3 Hz (corresponding to an average sliding velocity of approximately 0.1 m/s) to stabilize the changes in the coefficient of friction (CoF). In this study, tribological tests were conducted at 80 °C, referring to the condition under which the friction reduction effect of functionalized polymers occurred in past studies [7,36]. The calculated λ values ranged between 0.3 and 0.03, indicating testing across the mixed to boundary lubrication region as per the Hamrock-Dowson equation [37]. Each test, utilizing a new 3/8-inch diameter SiC ball with a roughness of 25 nm, lasted for 20 s at different frequencies. The changes in frequency range and respective sliding speeds are given in Table 3. The average steady-state CoF were determined for each sliding speed.

Furthermore, a wear test was performed using the same tribometer at 80 °C. A load of one hundred N was applied over a continuous sliding period of 20 min. The test involved a SiC ball with a 3/8-inch diameter, reciprocating over a stroke length of one mm at a frequency of 5 Hz. After the tribological tests, the surface of samples were thoroughly cleaned with heptane, and the wear profiles were analyzed using a white light interferometry (Rtec Instruments). The wear rates reported are the mean values, including standard deviations, derived from three repeated tests.

2.4. Computational method

To elucidate the influence of the functional group on the copolymer-surface interaction, we compared DMAEMA, constituting the functional part of the copolymer, and a shortened version of LMA, which composes the rest of the copolymer. The hydrocarbon tail of LMA was shortened from twelve to six carbon atoms to reduce the computational effort, mainly due to the large size of the simulation cell that would be required to contain the non-shortened molecule. The ball-and-stick representation of the two molecules is visible in Fig. 2.

The two structures are similar, both having the same C═O bond on the side attached to the carbon backbone of the copolymer, while the main difference is the presence of a N atom in DMAEMA as opposed to a simple hydrocarbon tail in LMA.

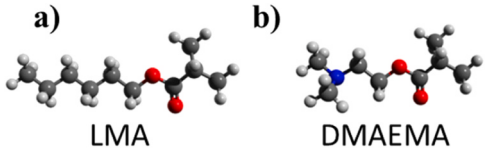

Fig. 2. Ball-stick representation of: (a) shortened LMA and (b) DMAEMA. C atoms are colored in gray, H in white, O in red and N in blue.

Table 3
Frequency ranges and sliding speeds during friction testing.

Step	1	2	3	4	5	6	7	8	9
Hz	5.00	4.50	4.00	3.50	3.00	2.75	2.50	2.25	2.0
m/s	0.150	0.135	0.120	0.105	0.090	0.083	0.075	0.068	0.060
Step	10	11	12	13	14	15	16	17	-
Hz	1.8	1.5	1.3	1.0	0.8	0.6	0.4	0.2	-
m/s	0.053	0.045	0.038	0.030	0.024	0.018	0.012	0.006	-

As substrate we first considered the dimer-reconstructed C (001) diamond surface, which is terminated by carbon dimers, where the carbon atoms form double bonds, giving rise to a surface morphology constituted by rows of 3-fold coordinated C atoms in a bonding configuration which is between sp^2 and sp^3 with a dangling bond. Even if the C(001) surface is different from the DLC surface on the large scale, the local bonding configuration may resemble that of the hydrogen-free DLC surface [38,39], since sp^2 layers are often observed on DLC after tribological tests [40], and non-planar C atoms with dangling bonds may also locally appear in the amorphous surface. Indeed the C(001) surface has been previously employed as a simple model for DLC in various works [41–44].

However, the real structure of amorphous DLC is very complex, due to the presence of a distribution of different bond angles and lengths.

To evaluate the applicability of our findings derived from the simplified C(001) surface model, the adsorption behavior of DMAEMA and LMA was further investigated on a more intricate model representing amorphous DLC.

To assess the generalizability of the results obtained for the simplified model of the C(001) surface, the adsorption of DMAEMA and LMA was studied also on a more realistic model of amorphous DLC. This DLC structure was built through molecular dynamics simulations using a machine-learning interatomic potential trained on *ab initio* data, specifically developed for amorphous carbon [45]. The simulations were carried out with the TurboGAP software [46–48]. Details on the procedure used to create the amorphous model are reported in the Supplementary Information.

To study the adsorption of LMA and DMAEMA on the different surfaces, it is necessary to sample a very large number of adsorption configurations, corresponding to different rotations and horizontal displacements of the molecules on the surface. For this purpose, we developed the program Xsorb [49], designed to carry out this "screening" procedure in an automatized way. In particular, Xsorb generates several configurations by changing the lateral and vertical position of the molecule with respect to the surface. For every position, different molecular rotation around the molecular axis and surface symmetry directions are considered. All these initial configurations are optimized until the energy and the forces become lower than the given threshold values. Only the most stable configurations are further optimized using smaller threshold values. In this way, the configurations with the highest statistical importance are identified among a large number of possibilities, thus avoiding relying just on the user choices, but still with a reasonable computational effort.

We applied `Xsorb` to screen more than a hundred initial configurations across the various molecule-substrate combinations. Different values of the initial molecule-surface separation were considered for every relative molecule-surface lateral position and orientation. This allowed us to sample both physisorption and chemisorption regimes. In the former regime, the molecule weakly interacts with the surface mainly through van der Waals interactions, and is trapped in a local energy minimum at a quite large distance from the surface; in the chemisorption regime, the molecule is more strongly bonded to the surface through covalent/ionic bonds and localizes at a smaller distance.

The DFT calculations were performed using the plane-waves, pseudopotential program included in the Quantum Espresso package [50]. The exchange correlation functional was described by the GGA-PBE approximation [51]. The plane wave basis set was truncated by a cutoff of 40 Ry for the kinetic energy and 320 Ry for the charge density. The Brillouin zone was sampled at the Γ point, which provides an accurate-enough k-point density thanks to the large size of the supercells used in this study. The calculations were performed with spin-polarization. A gaussian smearing of 0.02 Ry was also employed. The convergence thresholds used for the energy and force were 10^{-4}Ry and $10^{-3}\frac{\text{Ry}}{\text{Bohr}}$, respectively. For the crystalline C(001) surface, a simulation cell of 20.2 Å x 15.1 Å x 24.0 Å size was used, containing a diamond slab 7.8 Å thick, composed of 5 bilayers (reconstructed on both sides), and a vacuum region 16 Å thick to separate the slab from its periodic replicas along the (001) direction. The PBE surface energy of the dimer-reconstructed surface was carefully checked, obtaining an excellent agreement with the MaterialsProject database [52,53]. For the amorphous surface, a simulation cell of 18.8 Å x 18.8 Å x 24.0 Å size was used, containing a slab ~14 Å thick. To better capture the nonlocal, long-range interactions, which play an important role in molecular adsorption, we included van der Waals corrections with the Grimme-D2 scheme [54]. It has, in fact, been extensively shown that the PBE functional often underestimates the adsorption energy, especially for organic molecules on crystal surfaces[55,56].

3. Results

3.1. Friction test

To evaluate the tribological performance of copolymers containing varying functional group contents, friction tests were conducted using both undoped and Si DLCs. The measured friction coefficients as a function of the sliding velocity are presented in Fig. 3. For the undoped film (Fig. 3**a**), the presence of functional groups in the copolymer does not produce any significant change in the frictional behavior, which may indicate that all the copolymers weakly interact with the DLC surface.

The inclusion of Si dopants in the film altered this picture, and different friction behaviors were recorded for the different copolymers that were considered. As shown in Fig. 3**b** for Si-DLC 4.8 %, the CoF remained relatively unchanged for the non-functionalized PLMA and $PLMA_{83}$-*b*-$PDMAEMA_{17}$, while $PLMA_{95}$-*b*-$PDMAEMA_5$ exhibited a decrease in CoF, particularly at lower sliding speeds. This friction reduction became more consistent on Si-DLC 8.3 % and Si-DLC 14.4 % films, where the $PLMA_{95}$-*b*-$PDMAEMA_5$ produced a surprisingly low CoF of 0.04 in the lowest speed range. Notably, unlike other copolymers, the CoF for $PLMA_{83}$-*b*-$PDMAEMA_{17}$ did not decrease on the Si-DLC 14.4 % substrate. In fact, an increase in CoF was observed at low sliding speeds. This indicates that the addition of functional groups is effective in reducing friction on the Si-DLCs in the low-speed region, but an appropriate amount of functional groups is required to obtain an effective friction reduction.

3.2. Surface analysis

We analyzed the surface morphology of the different DLC films used in the tribology test through atomic force microscopy (AFM). In each panel of Fig. 4, we report the surface image acquired outside the wear trace as representative of the situation before the frictional test and three images acquired inside the wear trace after the tribological tests involving the three different considered copolymers. Overall, the surface topography outside the wear trace shows the characteristic nodular structure of DLCs. This does not change considerably inside the wear trace for the undoped substrate (Fig. 4**a**). On the contrary, particles of various sizes appear inside the wear traces of doped DLC. Especially on the Si-DLC 8.3 % and Si-DLC 14.4 % substrates, very large particles are observed when the friction test is performed with the $PLMA_{95}$-*b*-$PDMAEMA_5$.

A detailed analysis of the particles formed in the friction tests involving the $PLMA_{95}$-*b*-$PDMAEMA_5$ and the Si-DLC 8.3 % substrate is shown in Fig. 5. The tapping mode was employed to measure more accurate topography (Fig. 5**a, b**) and the contact mode was utilized to calculate the lateral signal on the surface (Fig. 5**c, d**). The surface profile along the cross-section indicated by a blue line in Fig. 5**b** shows that the particle shape is bidimensional, with a thickness of about 17 nm and a very smooth surface (the roughness is about 0.5 nm). The observed particle formation suggests these particles are patches of tribofilms. It should also be noted that the combination of the $PLMA_{95}$-*b*-$PDMAEMA_5$

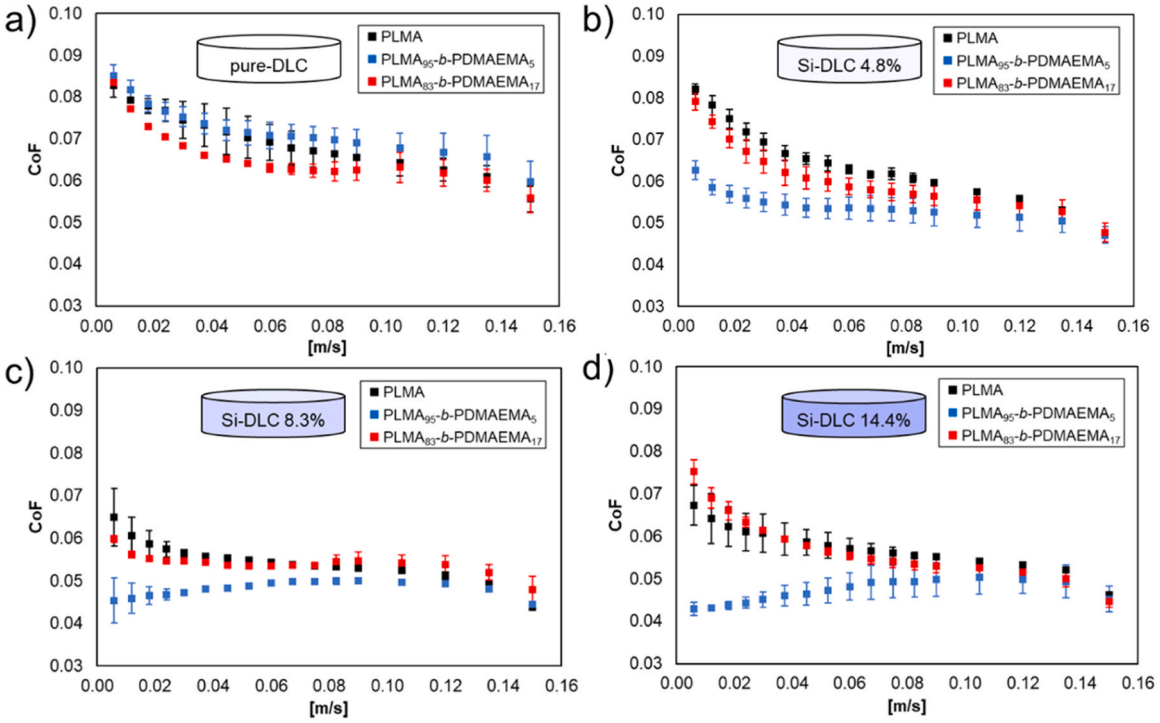

Fig. 3. Friction properties of copolymers with three different amounts of functional groups on pure-DLC (a), and doped films with different concentrations of Si atoms (b-d) with the standard deviation.

and Si-DLC 8.3 % or Si-DLC 14.4 % substrates produces large particles that showed a significant friction reduction effect. Fig. 5**c, d** display the outcomes of lateral signal measurements conducted in contact mode on a patch of tribofilm subjected to testing with $PLMA_{95}$-*b*-$PDMAEMA_5$ on Si-DLC 8.3 %. The surface height and signal force results depicted in Fig. 5**d** correspond to the blue line in Fig. 5**c**. The comparison of trends in lateral force and friction coefficient can be made by observing the increase or decrease in the lateral signal [18,57]. The AFM measurements produced results with different scans from left to right (forward) and right to left (backward). However, it is important to note that the signal derived from topography maintains the same tilt direction as the cantilever, regardless of the scan direction. Therefore, by subtracting the lateral forward signal from the lateral backward signal, the impact of topography was minimized. The results reveal that the lateral signal on the tribofilm patch remains consistently low and stable, suggesting that the friction reduction attributed to Si-DLC 8.3 % is a direct result of the formation of the tribofilm. The tribofilm acts as a protective layer that reduces direct contact between the sliding surfaces, thereby minimizing friction. The stable and low lateral signal further implies that the tribofilm provides a consistent and uniform shear resistance, which is critical for maintaining low friction over time.

3.3. Wear test

A wear test was conducted to assess the wear characteristics of functionalized polymers. Given the observed aggregation and poor reactivity of $PLMA_{83}$-*b*-$PDMAEMA_{17}$ with Si-DLC, this study conducted a comparative wear performance analysis between PLMA and $PLMA_{95}$-*b*-$PDMAEMA_5$. Fig. 6**a** presents the average CoF values for one minute just before the wear test concluded, along with the standard deviation from three repeated tests. The CoF for the entire 20 min during the wear test is shown in Fig. S4 in the Supplementary Information. The results indicate no discernible difference between the two polymers on pure-DLC, while on Si-DLC, the CoF decreased with the use of the functionalized polymer. Fig. 6**b** depicts the wear rates of all DLCs after wear testing from three repetitions. In the case of undoped DLC, the wear ratio remains unaffected by the type of polymer used. However, as the silicon concentration within the DLC film increases, a improvement in wear performance was observed in the presence of functionalized polymers. This suggests that the increased Si content enhances the interaction with $PLMA_{95}$-*b*-$PDMAEMA_5$, promoting the formation of a tribofilm that protects the surface contact. At Si-DLC 14.4 %, the wear rate increased even in the presence of $PLMA_{95}$-*b*-$PDMAEMA_5$. This is likely due to the increase in hardness attributed to SiC formation in the Si-DLC. As reported in other studies [58,59], the generation of hard debris particles during wear may contribute to the observed increase in wear rate. Analysis of the wear depths (all exceeding 50 nm) suggests that the thin surface oxide layer (approximately 1.2 nm) on the Si-DLC films was readily removed during the wear test. This indicates that the functionalized polymer lubricant likely interacted with the underlying Si-DLC film from the beginning of the experiment.

3.4. Dynamic light scattering

The friction test revealed that for Si-doped DLCs, the addition of $PLMA_{95}$-*b*-$PDMAEMA_5$ led to a significant reduction in the CoF in the low-speed range, while the $PLMA_{83}$-*b*-$PDMAEMA_{17}$ did not produce a reduction of the CoF, but rather an increase in the low-speed region (Fig. 3). This indicates that a specific amount of functional groups is necessary to effectively reduce friction on Si-DLCs. Since this difference could be due to the aggregation of the copolymers, DLS was used to measure the size of the polymer particles in the solution. The size measured for $PLMA_{83}$-*b*-$PDMAEMA_{17}$ was 232 nm, which was larger than the size of 146 nm measured for $PLMA_{95}$-*b*-$PDMAEMA_5$, indicating that the first copolymer is more aggregated than the second. From this result, it can be deduced that friction reduction was not observed at a higher concentration of functional groups, as the aggregation contributes to the reduction of functional groups available for the interaction between the dopants and the substrate (Fig. 7).

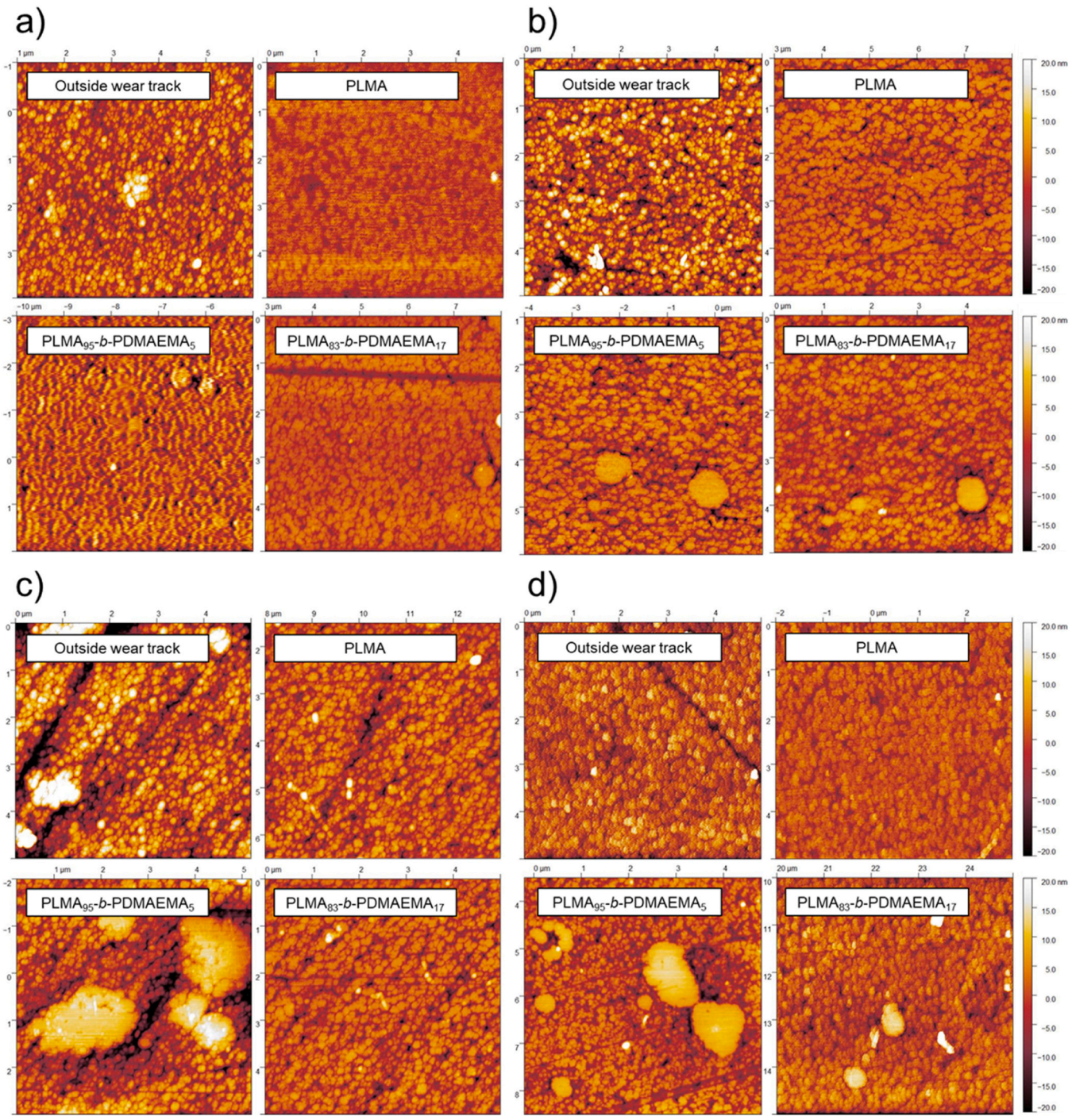

Fig. 4. Topography of the undoped DLC (a) and doped DLC with Si concentrations of 4.8 % (b), 8.3 % (c) and 14.4 % (d).

3.5. First principles calculations

The first essential step for the formation of a tribofilm by molecular additives is represented by their adsorption on the surface. Indeed, once the molecules adsorbed, they can prevent a direct solid-solid contact by steric hindrance or by forming tribofilms that decrease the interfacial adhesion and friction. To get insights into the adsorption properties of the functionalized additives on doped DLC, we analyzed the molecule-surface interactions by DFT calculations. As explained in the methodological section, the local bonding configuration was studied by considering the dimer-reconstructed C(001) diamond surface, both undoped and silicon-doped (8.3 % coverage). Previous DFT calculations revealed that the most favorable location for the dopant in the C(001) surface is a substitutional site in the dimer [28]. The experimental analysis of Si-DLC films corroborates this result, identifying the Si dopant surrounded by C-sp^2 atoms as the prevailing configuration [60].

The most stable adsorption configurations for each molecule on each substrate in the two adsorption regimes are reported in Fig. 8. For each configuration we provide the adsorption energy E_{ads} defined as:

$$E_{ads} = E_{slab+mol} - E_{slab} - E_{mol}$$

where $E_{slab+mol}$ is the energy of the configuration with the molecule adsorbed over the surface, E_{slab} is the energy of the substrate without the molecule, and E_{mol} is the energy of the isolated molecule (in vacuum). A

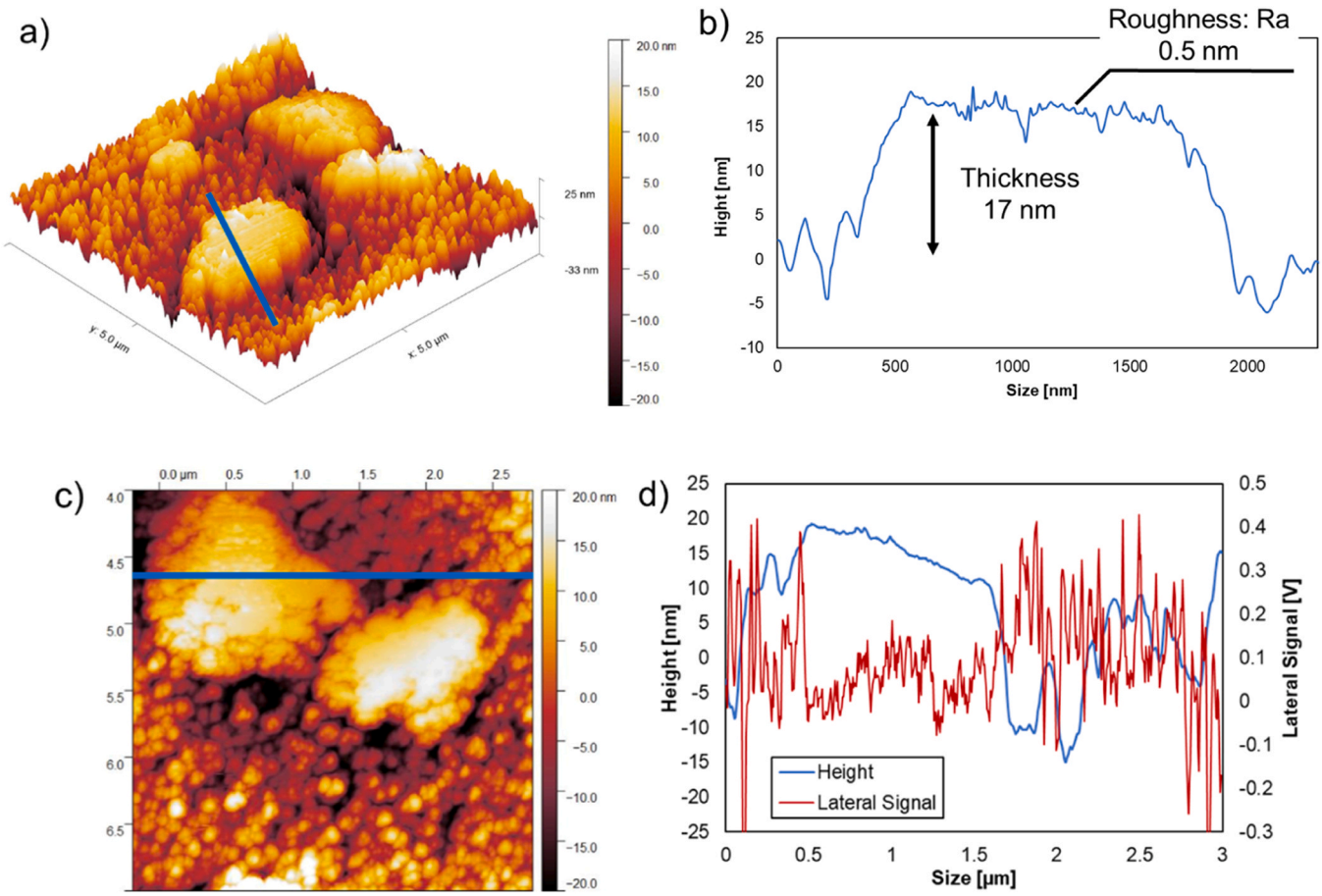

Fig. 5. Tapping mode: (a) Topography of wear trace after friction test with $PLMA_{95}$-*b*-$PDMAEMA_5$ on Si-DLC 8.3 % and (b) cross section on blue line, Contact mode: (c) Topography of wear trace after friction test with $PLMA_{95}$-*b*-$PDMAEMA_5$ on Si-DLC 8.3 % and (d) lateral signal on blue line.

negative value for E_{ads} indicates that the adsorption process is accompanied by an energy gain (equal to $-E_{ads}$).

Both LMA and DMAEMA have a stable physisorption configuration on undoped diamond (Fig. 8**a,b**), with almost identical adsorption energies. The inclusion of a Si-dopant in the surface does not affect the adsorption of LMA, which is physisorbed (Fig. 8**c**) with an energy gain equivalent to that on the undoped surface. A completely different behavior is observed for DMAEMA: in this case the molecular attraction is enhanced by the presence of the Si dopant and during the relaxation process at T = 0 K the molecule gets closer and closer to the surface until a chemical bond is established between the N and Si atoms (Fig. 8**d**). Notably, the initial molecule-surface separation is the same as that considered for the clean surface, but while in this case the molecule is trapped in the physisorption minimum of Fig. 8**b**, the presence of the Si dopant makes this local minimum disappear and promotes a stronger molecular binding with a high associated energy gain of 2.39 eV. This comparison shows that only the combination of DMAEMA and Si-doped surface produces an increase in chemical reactivity, with the formation of a bond and a significant change in adsorption energy, while all the other three combinations result in weak physisorption with almost identical adsorption energies, mainly due to van der Waals interactions.

The generalizability of the results obtained for the crystalline C(001) surface was studied by considering a model of the amorphous surface, including the substitutional Si dopant in two regions with different morphology: one with a planar, graphitic-like environment, and the other with a non-planar environment. More details and images of the two surface structures are reported in the Supplementary Information.

The adsorption structures and energies of DMAEMA and LMA with the substitutional Si in the two environments obtained with *ab initio* calculations are reported in Fig. 9**.** Even if the adsorption energy varies significantly from the values obtained for the crystalline C(001) surface, the trend between DMAEMA and LMA is maintained. DMAEMA always forms a N-Si bond, as opposed to LMA which does not bond to the surface. The energy difference between DMAEMA and LMA for the same local environment of the substitutional Si is also of the order of 1 eV, showing a non-negligible energy gain from the formation of the N-Si bond.

Even if this study on amorphous DLC is still limited to two local surface environments, and a much more extensive computational study would be needed to capture the variability of the amorphous surface and to accurately reproduce the real DLC used in the experiments, these results show that the qualitative behavior is consistent across different surface environments, providing good indication that the N-Si bond formation is not specific only to the simple model of the crystalline C (001) surface, but is relevant also to the amorphous DLC surface.

A more in-depth study on the N-Si bond that anchors DMAEMA to the substrate was performed for the crystalline C(001) surface by analyzing the charge redistribution that takes place upon the formation of the bond between the molecule and the heterodimer. Before the formation of the bond, the N atom in DMAEMA showed a negative partial charge (−0.20e), while the Si atom in the substrate showed a positive one (+0.44e) due to a charge transfer to the three neighboring C atoms (−0.20e on each of the two C atoms of the atomic plane below the dimer, and −0.12e on the C atom of the Si-C heterodimer). The presence of these partial charges of opposite sign on N and Si gives rise the electrostatic attraction that promotes the molecular attachment to the surface in the absence of any energy barrier. When the bond is formed, a charge transfer from N to the surface is observed, since N becomes less

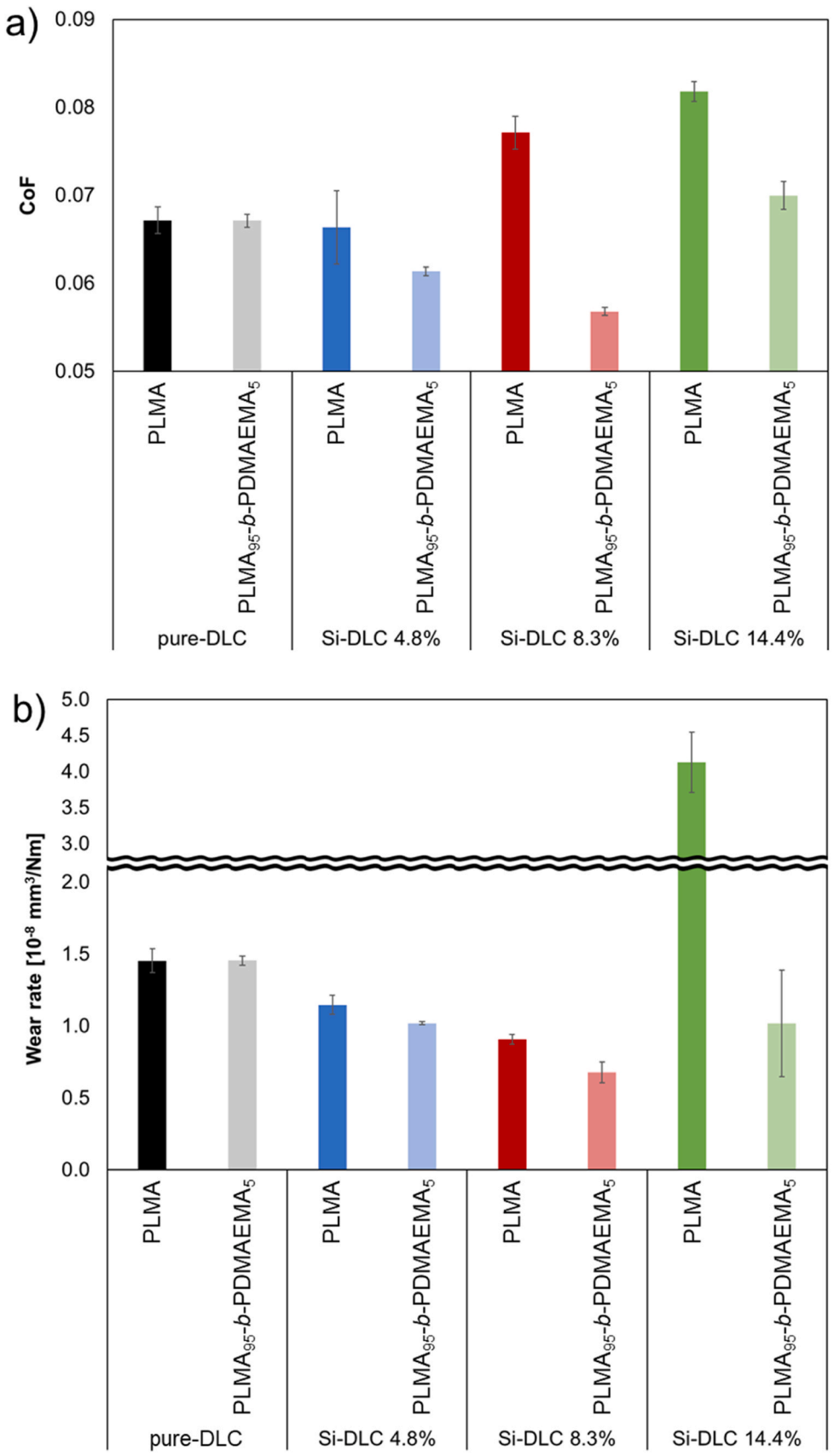

Fig. 6. (a) CoF during the last minute of the wear test and (b) Wear rate after wear testing. The average CoF and wear rate with the corresponding standard deviation was computed from three repeated tests.

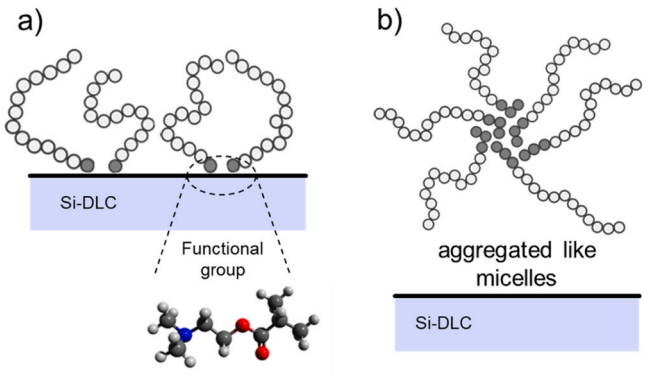

Fig. 7. Schematic representation of the functionalized copolymer with the $PLMA_{95}$-*b*-$PDMAEMA_5$ (a) and the $PLMA_{83}$-*b*-$PDMAEMA_{17}$ (b).

negative (−0.13). Simultaneously, the C atom in the heterodimer gains charge, reaching the value −0.38, while the Si atom undergoes a further charge loss, becoming significantly positive (+1.13).

The charge density difference associated to the formation of this bond, visible in Fig. 10, suggests the formation of a dative bond, where the charge is donated by the N atom, with a consequent disappearance of the lone pair located on this atom when in the isolated molecule (the corresponding charge depletion is visible Fig. 10**a**, which displays a high value of the charge difference isosurface).

The formation of a N-Si dative bond has been extensively described by previous experimental and computational studies [61–65] for molecules with a similar structure to DMAEMA, such as TMA (tri-methyl ammonium) and *N,N*-Dimethylbutylamine. All these studies were performed for the 2 × 1 dimer-reconstructed Si (001) surface, instead of the Si-doped C (001) surface, but the local N-Si interaction is most likely similar. The partial ionic nature of the N-Si bond, being the Si atom depleted by further charge accumulation on the C atom of the heterodimer, is also in agreement with the results for the pure Si dimer-reconstructed surface [61]. Moreover, the charge accumulation on the C of the heterodimer, forming a very reactive dangling bond (Fig. 10**c**) has also been discussed in previous works: the formation of the N-Si bond seems, in fact, to promote a net transfer of charge from the molecule to the surface, resulting in the appearance of a dangling bond on the other atom of the heterodimer [62].

In addition to the above-described formation of N-Si bond that allows for DMAEMA chemisorption on the substrate, an O-Si bond can be also established, as shown in the Supplementary Information. However, we do not believe that the formation of this bond is the mechanism that gives rise to the observed improvement of the tribological properties obtained with polymer functionalization, because the same O-Si bond

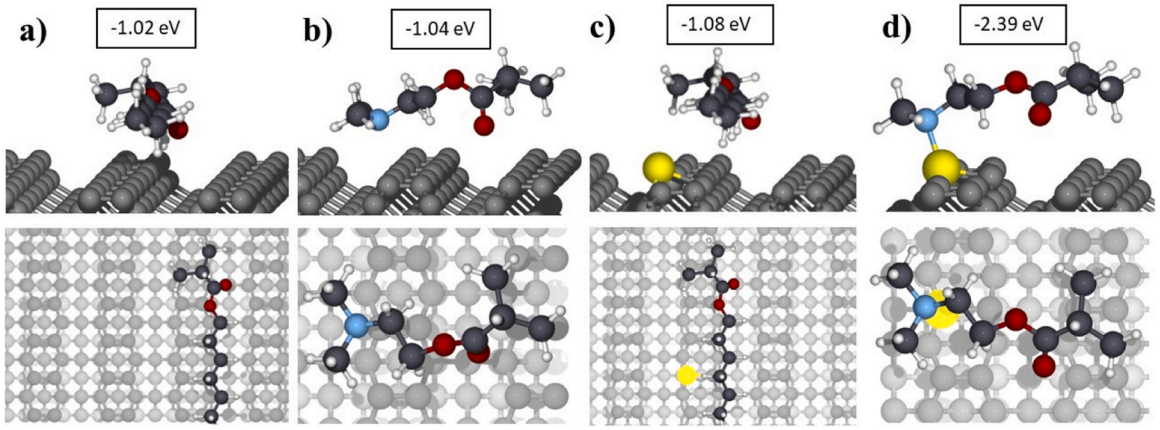

Fig. 8. Most stable adsorption configurations seen from lateral and top view of LMA (a,c) and DMAEMA (b,d) on undoped and Si-doped diamond. For the hydrocarbon tail of LMA only physisorption configurations exist, while for DMAEMA a chemical bond between nitrogen and silicon of the Si-doped surface is formed (d). The adsorption energy of each configuration is reported in the rectangular box. The atoms are colored as follows: grey for carbon in the substrate, black for carbon in the molecule, white for hydrogens, yellow for silicon, red for oxygen and blue for nitrogen.

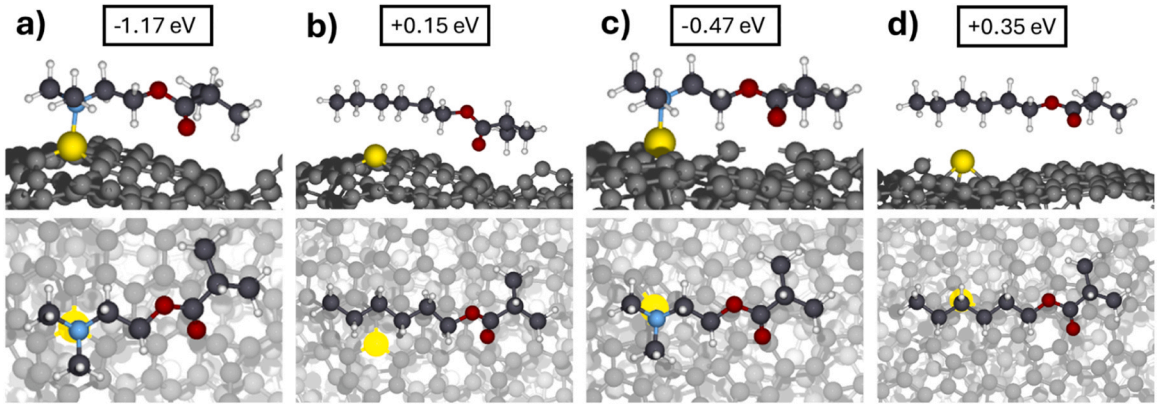

Fig. 9. Comparison of adsorption configurations for DMAEMA on planar (a) and non-planar (c) regions, and LMA on planar (b) and non-planar (d) regions of the DLC surface. DMAEMA forms a N-Si chemical bond on both regions, while LMA is not attracted by the surface. The adsorption energy of each configuration is reported in the rectangular box. The atoms are colored as follows: grey for carbon in the substrate, black for carbon in the molecule, white for hydrogens, yellow for silicon, red for oxygen and blue for nitrogen.

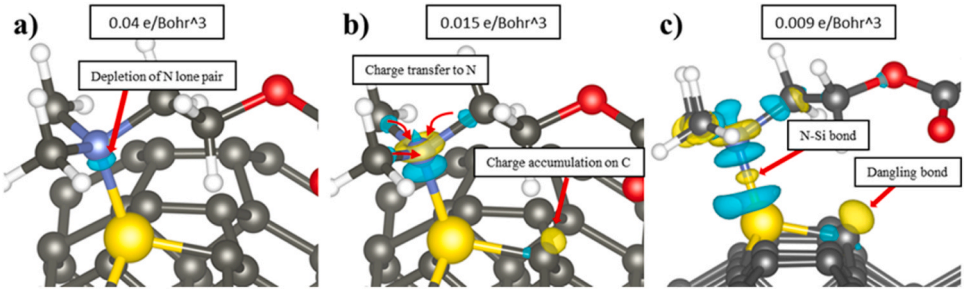

Fig. 10. Charge density difference for the adsorption of DMAEMA on Si-doped diamond. Progressively lower values of the isosurface are represented. Charge accumulation (depletion) is represented in yellow (blue). A strong depletion below the nitrogen in a) is associated to the formation of a dative bond from the nitrogen lone pair. In b) the charge transfer from N is partially compensated by a transfer from the neighboring C molecular atoms, and the charge accumulation on the C of the heterodimer becomes visible. In c) the formation of the N-Si bond is manifested through a charge accumulation in the middle of the bond, and the formation of a dangling bond above the C of the heterodimer becomes apparent.

can be formed also with LMA, as shown in the Supplementary Information. Moreover, the oxygen in both molecules is not part of the molecule termination but is instead located on the side of the main polymer backbone. Thus, when the polymer is immersed into the PAO oil during sliding, the oxygen atoms may have a much lower chance of getting close enough to the surface to form a bond.

4. Conclusion

This study demonstrates the achievement of consistent wear and friction reduction, even under the boundary lubrication regime, through synergistic chemical modifications in both the polymer lubricant additive and the substrate film. Additionally, surface analysis utilizing AFM has unveiled that $PLMA_{95}$-*b*-$PDMAEMA_5$ forms patches of tribofilm on the Si-DLC surface.

To gain insights into the first step of tribofilm formation, we performed *ab initio* calculations of molecular adsorption for the molecules that constitute the copolymer. Both undoped and Si-doped crystalline diamond surfaces, and Si-doped amorphous surfaces were considered. The results show that on the undoped surface both the functional and non-functional molecules are weakly physisorbed. On the contrary, the presence of a Si dopant highly increases the surface attraction for the DMAEMA molecule and promotes its spontaneous chemisorption through the formation of a N-Si bond, which is observed both on the crystalline and amorphous model of the DLC. A detailed analysis of the electronic mechanisms for this bond formation is provided and its key role in the early stage of tribofilm formation is discussed. Further investigations on the structure and composition of the tribofilm will be the subject of a forthcoming article, which will also include molecular dynamic simulations of tribofilm formation, the first important step of which consists in the process of molecular chemisorption addressed in the present work.

Overall, our study provides valuable insights into the tribological properties of functionalized copolymers on DLCs and highlights the importance of the Si doping of the substrate, in combination with the inclusion of an appropriate amount of functional groups into the copolymer, in achieving effective friction reduction and wear reduction. These findings may contribute to the development of advanced films with enhanced frictional properties for various applications in industries such as automotive and manufacturing.

Statement of originality

I confirm that this paper is original and it has not been published previously and it is not under consideration elsewhere. Maria Clelia Righi, on behalf of all authors.

CRediT authorship contribution statement

Takeru Omiya: Writing – review & editing, Writing – original draft, Visualization, Validation, Software, Project administration, Methodology, Investigation, Formal analysis, Data curation, Conceptualization. **Albano Cavaleiro:** Supervision, Resources, Funding acquisition. **Arménio C. Serra:** Resources, Funding acquisition. **Enrico Pedretti:** Writing – review & editing, Writing – original draft, Visualization, Validation, Software, Methodology, Investigation, Formal analysis, Data curation, Conceptualization. **Manuel Evaristo:** Methodology, Data curation. **Maria Clelia Righi:** Writing – review & editing, Visualization, Validation, Supervision, Software, Resources, Project administration, Methodology, Investigation, Funding acquisition, Formal analysis, Data curation, Conceptualization. **Jorge F.J. Coelho:** Writing – review & editing, Supervision, Resources, Project administration, Methodology, Investigation, Conceptualization. **Fabio Ferreira:** Writing – original draft, Supervision, Resources, Project administration, Funding acquisition, Conceptualization.

Declaration of Competing Interest

The authors declare that they have no known competing financial interests or personal relationships that could have appeared to influence the work reported in this paper.

Data Availability

Data will be made available on request.

Acknowledgments

This research is supported by national funding from FCT – Fundação para a Ciência e a Tecnologia, under projects UIDB/00285/2020 and LA/P/0112/2020, SmartHyLub (2022.05603. PTDC), iLub (2022.15609. UTA) and by the Taiho Kogyo Tribology Research Foundation (Grant No. 22A25). These results are part of the "Advancing Solid Interface and Lubricants by First Principles Material Design (SLIDE)" project that has received funding from the European Research Council (ERC) under the European Union's Horizon 2020 research and innovation program (Grant agreement No. 865633).

Conflict of interest

The authors have no competing interests.

Appendix A. Supporting information

Supplementary data associated with this article can be found in the online version at doi:10.1016/j.triboint.2024.110183.

References

[1] Verstrate G., Struglinski M.J. Polymers as lubricating-oil viscosity modifiers 1991.
[2] Nassar AM. The behavior of polymers as viscosity index improvers. Pet Sci Technol 2008;26:514–22.
[3] Mohamad SA, Ahmed NS, Hassanein SM, Rashad AM. Investigation of polyacrylates copolymers as lube oil viscosity index improvers. J Pet Sci Eng 2012; 100:173–7.
[4] Covitch MJ, Trickett KJ. How polymers behave as viscosity index improvers in lubricating oils. Adv Chem Eng Sci 2015;05:134–51.
[5] Bhattacharya P, Ramasamy US, Krueger S, Robinson JW, Tarasevich BJ, Martini A, et al. Trends in thermoresponsive behavior of lipophilic polymers. Ind Eng Chem Res 2016;55:12983–90.
[6] van Ravensteijn BGP, Bou Zerdan R, Seo D, Cadirov N, Watanabe T, Gerbec JA, et al. Triple function lubricant additives based on organic-inorganic hybrid star polymers: friction reduction, wear protection, and viscosity modification. ACS Appl Mater Interfaces 2019;11:1363–75.
[7] Muller M, Topolovec-Miklozic K, Dardin A, Spikes HA. The design of boundary film-forming PMA viscosity modifiers. Tribology Trans 2006;49:225–32.
[8] Fan J, Müller M, Stöhr T, Spikes HA. Reduction of friction by functionalised viscosity index improvers. Tribology Lett 2007;28:287–98.
[9] Gmür TA, Mandal J, Cayer-Barrioz J, Spencer ND. Towards a Polymer-Brush-Based friction modifier for oil. Tribology Lett 2021;69:124.
[10] Delamarre S, Gmür T, Spencer ND, Cayer-Barrioz J. Polymeric friction modifiers: Influence of anchoring chemistry on their adsorption and effectiveness. Langmuir 2022;38:11451–8.
[11] Sappok A, Rodriguez R, Wong V. Characteristics and effects of lubricant additive chemistry on ash properties impacting diesel particulate filter service life. SAE Int J Fuels Lubr 2010;3:705–22.
[12] Grill A. Diamond-like carbon: state of the art. Diam Relat Mater 1999;8:428–34.
[13] Erdemir A, Donnet C. Tribology of diamond-like carbon films: recent progress and future prospects. J Phys D: Appl Phys 2006;39:R311–27.
[14] Podgornik B, Vižintin J. Tribological reactions between oil additives and DLC coatings for automotive applications. Surf Coat Technol 2005;200:1982–9.
[15] Cruz R, Rao J, Rose T, Lawson K, Nicholls JR. DLC–ceramic multilayers for automotive applications. Diam Relat Mater 2006;15:2055–60.
[16] Kano M. Diamond-like carbon coating applied to automotive engine components. Tribology Online 2014;9:135–42.
[17] Kano M, Yasuda Y, Okamoto Y, Mabuchi Y, Hamada T, Ueno T, et al. Ultralow friction of DLC in presence of glycerol mono-oleate (GNO). Tribology Lett 2005;18: 245–51.
[18] Vengudusamy B, Green JH, Lamb GD, Spikes HA. Tribological properties of tribofilms formed from ZDDP in DLC/DLC and DLC/steel contacts. Tribology Int 2011;44:165–74.
[19] Kalin M, Velkavrh I, Vižintin J, Ožbolt L. Review of boundary lubrication mechanisms of DLC coatings used in mechanical applications. Meccanica 2008;43: 623–37.
[20] Kalin M, Vižintin J, Barriga J, Vercammen K, Acker Kv, Arnšek A. The effect of doping elements and oil additives on the tribological performance of boundary-lubricated DLC/DLC contacts. Tribology Lett 2004;17:679–88.
[21] Vetter J. 60 years of DLC coatings: Historical highlights and technical review of cathodic arc processes to synthesize various DLC types, and their evolution for industrial applications. Surf Coat Technol 2014;257:213–40.
[22] Barriga J, Kalin M, Acker KV, Vercammen K, Ortega A, Leiaristi L. Tribological performance of titanium doped and pure DLC coatings combined with a synthetic bio-lubricant. Wear 2006;261:9–14.
[23] Kržan B, Novotny-Farkas F, Vižintin J. Tribological behavior of tungsten-doped DLC coating under oil lubrication. Tribology Int 2009;42:229–35.
[24] Zahid R, Masjuki HH, Varman M, Mufti RA, Kalam MA, Gulzar M. Effect of lubricant formulations on the tribological performance of self-mated doped DLC contacts: a review. Tribology Lett 2015;58:32.
[25] Omiya T, Fontes M, Vuchkov T, Cruz S, Cavaleiro A, Ferreira F. Tribological performance of Gd-DLC and Eu-DLC coatings in the presence of synthetic oils containing ionic liquid additives. Tribology Lett 2023;71:65.
[26] Omiya T, Cavaleiro A, Figueiredo N, Gouttebaron R, Felten A, Ferreira F. Sustainable lubrication through Gd DLC films and ionic liquids for wear and corrosion resistance. Tribology Int 2024:110130.
[27] Evaristo M, Azevedo R, Palacio C, Cavaleiro A. Influence of the silicon and oxygen content on the properties of non-hydrogenated amorphous carbon coatings. Diam Relat Mater 2016;70:201–10.
[28] Kajita S, Righi MC. Insigths into the tribochemistry of silicon-doped carbon-based films by ab initio analysis of water–surface interactions. Tribology Lett 2016;61:17.
[29] Ayestarán Latorre C, Ewen JP, Dini D, Righi MC. Ab initio insights into the interaction mechanisms between boron, nitrogen and oxygen doped diamond surfaces and water molecules. Carbon 2021;171:575–84.
[30] Wang J, Pu J, Zhang G, Wang L. Tailoring the structure and property of silicon-doped diamond-like carbon films by controlling the silicon content. Surf Coat Technol 2013;235:326–32.
[31] Nakazawa H, Kamata R, Okuno S. Deposition of silicon-doped diamond-like carbon films by plasma-enhanced chemical vapor deposition using an intermittent supply of organosilane. Diam Relat Mater 2015;51:7–13.
[32] Robertson J. Diamond-like amorphous carbon. Mater Sci Eng: R: Rep 2002;37: 129–281.
[33] Ferrari AC, Robertson J. Raman spectroscopy of amorphous, nanostructured, diamond-like carbon, and nanodiamond. Philos Trans A Math Phys Eng Sci 2004; 362:2477–512.
[34] Cui W, Lai Q, Zhang L, Wang F. Quantitative measurements of sp3 content in DLC films with Raman spectroscopy. Surf Coat Technol 2010;205:1995–9.
[35] Omiya T, De Bon F, Vuchkov T, Serra A, Cavaleiro A, Coelho J, et al. Wear resistance by copolymers with controlled structure under boundary lubrication conditions. Lubr Sci 2024;36:1–8.
[36] Smeeth M, Spikes H, Gunsel S. Boundary film formation by viscosity index improvers. Tribology Trans 1996;39:726–34.
[37] Hamrock BJ, Dowson D. Ball Bearing Lubrication (The Elastohydrodynamics of Elliptical Contacts). J Lubr Technol 1981;104:279–81.
[38] Wang L-F, Ma T-B, Hu Y-Z, Wang H, Shao T-M. Ab initio study of the friction mechanism of fluorographene and graphane. J Phys Chem C 2013;117:12520–5.
[39] Zilibotti G, Corni S, Righi MC. Load-induced confinement activates diamond lubrication by water. Phys Rev Lett 2013;111:146101.
[40] Jiang DE, Carter EA. Carbon atom adsorption on and diffusion into Fe(110) and Fe (100) from first principles. Phys Rev B 2005;71:045402.
[41] Dag S, Ciraci S. Atomic scale study of superlow friction between hydrogenated diamond surfaces. Phys Rev B 2004;70:241401.
[42] Bai S, Xu J, Wang Y, Zhang Q, Tsuruda T, Higuchi Y, et al. Generation of “Graphene Arch-Bridge” on a diamond surface by Si doping: a first-principles computational study. J Phys Chem C 2020;124:26379–86.
[43] Tran NV, Righi M. Ab initio insights into the interaction mechanisms between H2, H2O, and O2 molecules with diamond surfaces. Carbon 2022;199:497–507.
[44] Liu Y, Zhang H, Luo Y, Wang L, Xiao C. Probing the low friction mechanism of hydrogen-free DLC film in oxygen and nitrogen environments by first-principles calculations and molecular dynamics simulation. Surf Coat Technol 2023;455: 129219.
[45] Wang Y, Fan Z, Qian P, Ala-Nissila T, Caro MA. Structure and pore size distribution in nanoporous carbon. Chem Mater 2022;34:617–28.
[46] Bartók AP, Payne MC, Kondor R, Csányi G. Gaussian approximation potentials: The accuracy of quantum mechanics, without the electrons. Phys Rev Lett 2010;104: 136403.
[47] Bartók AP, Kondor R, Csányi G. On representing chemical environments. Phys Rev B 2013;87:184115.
[48] Caro MA. Optimizing many-body atomic descriptors for enhanced computational performance of machine learning based interatomic potentials. Phys Rev B 2019; 100:024112.
[49] Pedretti E, Restuccia P, Righi MC. Xsorb: a software for identifying the most stable adsorption configuration and energy of a molecule on a crystal surface. Comput Phys Commun 2023;291:108827.
[50] Giannozzi P, Baroni S, Bonini N, Calandra M, Car R, Cavazzoni C, et al. QUANTUM ESPRESSO: a modular and open-source software project for quantum simulations of materials. J Phys Condens Matter 2009;21:395502.
[51] Perdew JP, Burke K, Ernzerhof M. Generalized gradient approximation made simple [Phys. Rev. Lett. 77, 3865 (1996). Phys Rev Lett 1997;78:1396.
[52] Jain A, Ong SP, Hautier G, Chen W, Richards WD, Dacek S, et al. Commentary: the materials project: a materials genome approach to accelerating materials innovation. APL Mater 2013;1:011002.
[53] Tran R, Xu Z, Radhakrishnan B, Winston D, Sun W, Persson KA, et al. Surface energies of elemental crystals. Sci Data 2016;3:160080.
[54] Grimme S. Semiempirical GGA-type density functional constructed with a long-range dispersion correction. J Comput Chem 2006;27:1787–99.
[55] Bjorkman T, Gulans A, Krasheninnikov AV, Nieminen RM. Are we van der Waals ready? J Phys Condens Matter 2012;24:424218.
[56] Liu W, Tkatchenko A, Scheffler M. Modeling adsorption and reactions of organic molecules at metal surfaces. Acc Chem Res 2014;47:3369–77.
[57] Vengudusamy B, Mufti RA, Lamb GD, Green JH, Spikes HA. Friction properties of DLC/DLC contacts in base oil. Tribology Int 2011;44:922–32.
[58] Bhushan B. Chemical, mechanical and tribological characterization of ultra-thin and hard amorphous carbon coatings as thin as 3.5 nm: recent developments. Diam Relat Mater 1999;8:1985–2015.
[59] Neuville S. Antiwear material criteria. JPJ Solids Struct 2009;3:33–42.
[60] Iseki T, Mori H, Hasegawa H, Tachikawa H, Nakanishi K. Structural analysis of Si-containing diamond-like carbon. Diam Relat Mater 2006;15:1004–10.
[61] Cao X, Hamers RJ. Silicon surfaces as electron acceptors: dative bonding of amines with Si(001) and Si(111) surfaces. J Am Chem Soc 2001;123:10988–96.
[62] Cao X, Hamers RJ. Formation of a surface-mediated donor−acceptor complex: coadsorption of trimethylamine and boron trifluoride on the silicon (001) surface. J Phys Chem B 2002;106:1840–2.
[63] Cao X, Hamers RJ. Interactions of alkylamines with the silicon (001) surface. Journal of Vacuum Science & Technology B: microelectronics and nanometer structures processing. Meas, Phenom 2002;20:1614–9.
[64] Carman AJ, Zhang LH, Liswood JL, Casey SM. Methylamine adsorption on and desorption from Si(100). J Phys Chem B 2003;107:5491–502.
[65] Ramírez LP, Fornefeld N, Bournel F, Kubsky S, Magnano E, Bondino F, et al. Trimethylamine probes isolated silicon dangling bonds and surface hydroxyls of (H,OH)-Si(001). J Phys Chem C 2022;126:2548–60.